Hindawi Publishing Corporation
International Journal of Distributed Sensor Networks
Volume 2013, Article ID 894780, 9 pages
http://dx.doi.org/10.1155/2013/894780

Research Article

Measurement Model for the Maximum Strain in Beam Structures Using Multiplexed Fiber Bragg Grating Sensors

Se Woon Choi,[1] Jihoon Lee,[1] Bo Hwan Oh,[2] and Hyo Seon Park[1]

[1] *Department of Architectural Engineering, Yonsei University, 134 Shincshon-dong, Seoul 120-749, Republic of Korea*
[2] *Daewoo Institute of Construction Technology, 60 Songjuk-dong, Suwon 440-210, Republic of Korea*

Correspondence should be addressed to Hyo Seon Park; hspark@yonsei.ac.kr

Received 12 July 2013; Revised 6 September 2013; Accepted 8 September 2013

Academic Editor: Hong-Nan Li

This study develops a strain measurement model for beam structures subjected to multiloading conditions by defining the strain-shape function and participation factors to overcome the limitations of strain measurements using fiber Bragg grating (FBG) strain sensors. Using the proposed model, the maximum strain in a beam is obtained by the sum of the strains caused by the different loadings acting separately. In this paper, the strain-shape functions for various loading and support conditions are provided, and a system of equations is defined to calculate the participation factors. Furthermore, the influence ratio is defined to identify the influence of each loading on the value of the total strain. The measurement model is applied to the monitoring of the maximum strain in a 4 m long steel beam subjected to two concentrated loads. For measurements during the test, seven FBG sensors and nine electric strain gauges (ESGs) were attached on the surface of the bottom flange. The experimental results indicate a good agreement between the estimated strains based on the model and the measured strains from ESGs. Furthermore, the dependency of the locations for the FBG sensors installed at the beam structure on the selection can be avoided using the measurement model.

1. Introduction

Structural members in buildings or infrastructures experience various loads, such as gravity-induced loads, earthquake, wind, or unexpected loads. To secure the safety of a structure, the maximum stresses in the members due to various loads must not exceed the allowable stress of a member [1, 2]. For this reason, strain-based structural health monitoring (SHM) has been widely used to assess the structural states of the members by sensing the maximum stresses [3–8].

Various types of point sensors, including fiber optic sensors and electric strain gauges (ESGs), are applied to measure the maximum stresses. However, point sensors used to measure strains can cover only a relatively small range of structural members because they can measure the strain only at a local point of a member. Thus, many difficulties exist when determining the maximum stress in a member with point sensors because the actual strain distribution of a member is nonuniform. In this case, the reliability of the safety of a member based on the measured maximum strain depends on the number and location of the sensors. However, when attempting to overcome these limitations, the number of sensors may not be increased to cover the entire length of a member because of practical problems related to maintenance and installation.

Various techniques to estimate the maximum strain based on the measured strains have been reported [5, 7] because the measured strains from point sensors cannot be directly considered when evaluating the safety of a member. To cover a relatively long length of a member, the average strains from long-gauge fiber optic sensors (LGFOSs) or vibrating wire strain sensors (VWSGs) have been used to estimate the maximum strains of a member subjected to a single loading condition. However, the techniques are rather impractical because structural members in real building structures or infrastructures are subjected to multiple loading conditions.

Considering the limits of point sensors and long-gauge sensors, fiber Bragg grating (FBG) strain sensors are suitable for measuring the maximum strain of a beam. Although an FBG sensor is a point sensor with a relatively short-gauge length, it can measure the maximum strains with a minimum

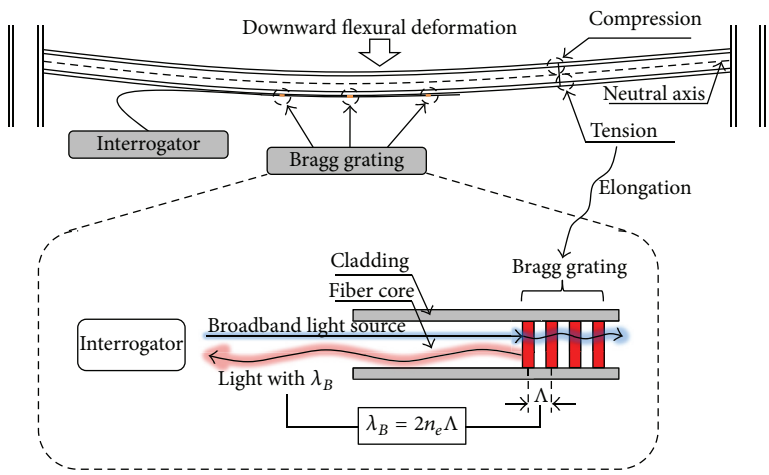

Figure 1: Measurement principle of the strain using an FBG sensor.

number of sensors because of the multiplexing technology in FBG [9]. Multiplexing is a method by which multiple signals are combined into one signal, and only a single cable suffices for a certain number of sensors. In addition, FBG strain sensors have high resolution and are convenient to install compared to long-gauge sensors.

However, to date, no research regarding point sensors, including FBG sensors, has been reported on the measurement or sensing method for the maximum strains in a structural member subjected to real multiple loading conditions. Therefore, in this paper, a maximum strain measurement model based on point sensors is developed for the FBG sensor to be applied to find the maximum strain in a steel beam structure subjected to multiple loading conditions. In addition to the maximum strain, a distribution of the strains along the length of a member is provided by the measured local strains from the minimum number of FBG sensors. To evaluate the performance of the model, an experiment has been conducted on a 4 m long steel beam to compare the maximum strain directly obtained from ESGs and the maximum strain from the model with the strains measured from FBG sensors.

2. FBG Sensors

In FBG sensors, a Bragg grating is introduced to the core of a fiber [10]. If the broadband light source collides against the Bragg grating, a light with a particular wavelength, called the Bragg wavelength λ_B, satisfying the relationship shown in (1) is reflected:

$$\lambda_B = 2n_e\Lambda, \tag{1}$$

where Λ is the period of Bragg grating and n_e is the effective refractive index. Because the Bragg grating period varies according to the elongation, a strain can be calculated by detecting the change of the Bragg wavelength that reflects an elongation.

As shown in Figure 1, the longitudinal strain of a beam member subjected to multiple loadings can be measured by typical FBG sensors attached to the face of the member. Especially from the aspect of SHM, the multiplexing technology in an FBG sensor makes strain-based SHM more reliable and practical because of the convenience with which such sensors can be managed and installed. A variety of applications can be found in the field of SHM, including building, civil, and infrastructure [11–15].

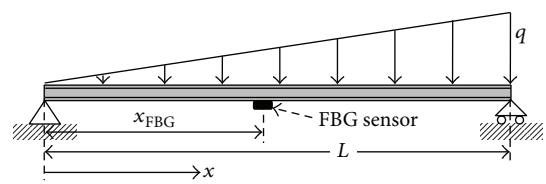

Figure 2: Simply supported beam subjected to a linearly varying load.

3. Maximum Strain Measurement Model

In this paper, the strain measurement model is presented to estimate the maximum strain of a beam structure using local strains measured from FBG sensors. For a beam structure subjected to multiple loading conditions simultaneously, the total strain at a specific point can be found by superimposing the strains due to separate loadings. However, to find the maximum strain of a beam structure instead of the strain value at a point, the deformed shape caused by the multiple loadings must be defined by superimposing the distribution shape of the strains along the length of a beam for each loading separately. The total strain at an arbitrary point in a beam structure can be estimated using the deformed shape.

3.1. Shape Function for the Distribution of Strains Caused by a Single Load. Based on general concepts in engineering mechanics, as shown in Figure 2, the longitudinal strain $\varepsilon(x)$ of a beam subjected to a linearly varying distributed load of

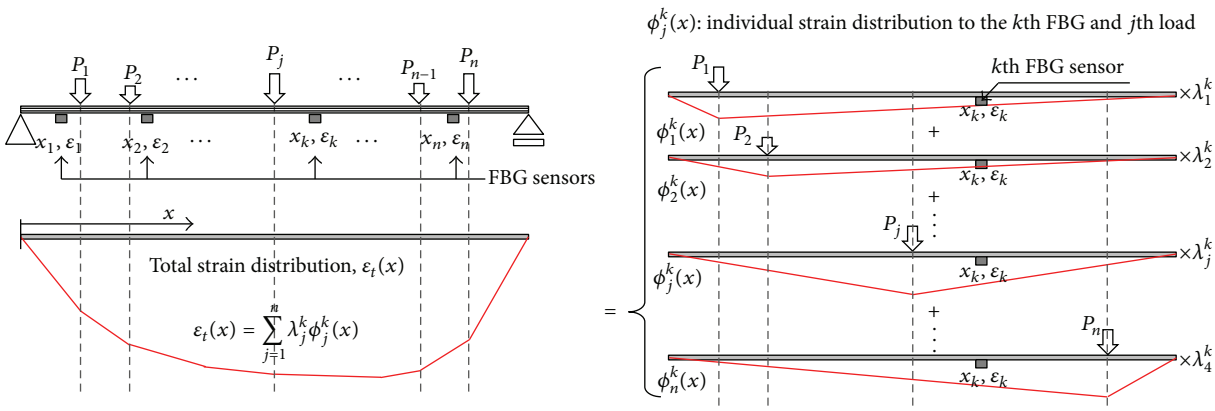

FIGURE 3: Decomposition of the strain distribution caused by multiple loadings into individual effects.

q can be expressed as a function of the distance x from the left-hand support:

$$\varepsilon(x) = \frac{M(x)}{EZ}, \tag{2}$$

where $M(x)$ is the bending moment, E is the modulus of elasticity, Z is the elastic section modulus, and L is the length of the beam. For a FGB sensor installed at a length of x_{FBG} in Figure 2, the strain measured from the FBG strain sensor ε_{FBG} is expressed as

$$\varepsilon_{\text{FBG}} = \frac{1}{EZ}\left(\frac{qL}{6}x_{\text{FBG}} - \frac{q}{6L}x_{\text{FBG}^3}\right). \tag{3}$$

From (3), the intensity of the distributed load q can be expressed as

$$q = \frac{2EZL\varepsilon_{\text{FBG}}}{x_{\text{FBG}}\left(L^2 - x^2{}_{\text{FBG}}\right)}. \tag{4}$$

Then, the general form for the longitudinal $\varepsilon(x)$ at an arbitrary point x can be defined by

$$\varepsilon(x) = \varepsilon_{\text{FBG}}\frac{x\left(L^2 - x^2\right)}{x_{\text{FBG}}\left(L^2 - x^2{}_{\text{FBG}}\right)} = \varepsilon_{\text{FBG}}\phi(x), \tag{5}$$

where $\phi(x)$ is defined as a shape function for the distribution of strains along the length of the beam. The strain-shape function $\phi(x)$ for the distribution of strains in (5) depends on the loading and support conditions of a beam structure. For convenience, nine typical shape functions for the distribution of strains in beam structures subjected to various loading and support conditions are derived in Tables 1 and 2.

As given in (5), the general form of $\varepsilon(x)$ for a beam subjected to a loading can be defined by the strain measured from an FBG sensor at an arbitrary location of x_{FBG} multiplied by the shape function $\phi(x)$ for the distribution of strains in Table 1.

3.2. Superposition of Shape Functions Caused by Multiple Loadings. For a beam structure subjected to n different point loadings of P_j ($j = 1$ to n) in Figure 3, the general form for the total strain $\varepsilon_t(x)$ of a beam at a distance x from the left-hand support can be expressed as the sum of the strains due to n different point loadings acting separately:

$$\varepsilon_t(x) = \sum_{j=1}^{n}\lambda_j^k\phi_j^k(x), \tag{6}$$

where λ_j^k is the participation factor for the jth strain-shape function $\phi_j^k(x)$. The superscript k in (6) is the FBG sensor number selected to calculate the strain-shape functions and the participation factors. The calculation of the participation factors is not dependent on the selection of an FBG sensor, as with other types of sensors. Thus, the value of the total strain in (6) does not vary with the selection of the FBG sensor used to calculate the factors.

For the kth FBG sensor selected for the calculation of the factors, a system of n simultaneous equations in (7) can be expressed in matrix notation as follows:

$$\begin{Bmatrix} \varepsilon_1 \\ \varepsilon_2 \\ \vdots \\ \varepsilon_j \\ \vdots \\ \varepsilon_n \end{Bmatrix} = \begin{bmatrix} \phi_{11}^k & \phi_{12}^k & \cdots & \phi_{1j}^k & \cdots & \phi_{1n}^k \\ \phi_{21}^k & \phi_{22}^k & \cdots & \phi_{2j}^k & \cdots & \phi_{2n}^k \\ \vdots & \vdots & \ddots & \vdots & \ddots & \vdots \\ \phi_{j1}^k & \phi_{j2}^k & \cdots & \phi_{jj}^k & \cdots & \phi_{jn}^k \\ \vdots & \vdots & \ddots & \vdots & \ddots & \vdots \\ \phi_{n1}^k & \phi_{n2}^k & \cdots & \phi_{nj}^k & \cdots & \phi_{nn}^k \end{bmatrix} \begin{Bmatrix} \lambda_1^k \\ \lambda_2^k \\ \vdots \\ \lambda_j^k \\ \vdots \\ \lambda_n^k \end{Bmatrix}, \tag{7}$$

where $\phi_{ij}^k = \phi_j^k(x_i)$ is the value of the jth strain-shape function at the position of x_i. Then, the participation factors can be found as the solution to (7):

$$\left\{\lambda^k\right\} = \left[\phi^k\right]^{-1}\left\{\varepsilon_{\text{FBG}}\right\}, \tag{8}$$

where $\{\lambda^k\}$ is a column vector of the participation factors, $[\phi^k]$ is a square matrix of ϕ_{ij}^k, and $\{\varepsilon_{\text{FBG}}\}$ is a column vector of the measured strains. Then, using the total strain obtained by the superposition of n shape functions for strains due to the multiple loadings in (6), the location for the maximum

Table 1: Distributional strain-shape function $\phi(x)$: simply supported beam.

Loading condition	Condition of FBG sensor location	$\phi(x)$
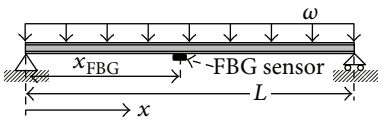	$0 < x_{FBG} < L$	$\dfrac{x(L-x)}{x_{FBG}(L-x_{FBG})}$
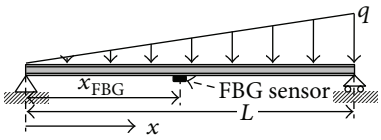	$0 < x_{FBG} < L$	$\dfrac{x(L^2-x^2)}{x_{FBG}(L^2-x^2{}_{FBG})}$
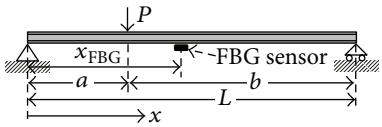	$0 < x_{FBG} \le a$	$\begin{cases} \dfrac{x}{x_{FBG}}, & (0 < x \le a), \\ \dfrac{a(L-x)}{bx_{FBG}}, & (a \le x \le L) \end{cases}$
	$a \le x_{FBG} < L$	$\begin{cases} \dfrac{bx}{a(L-x_{FBG})}, & (0 < x \le a), \\ \dfrac{L-x}{L-x_{FBG}}, & (a \le x \le L) \end{cases}$
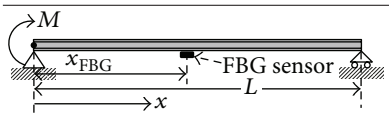	$0 \le x_{FBG} < L$	$\dfrac{L-x}{L-x_{FBG}}$
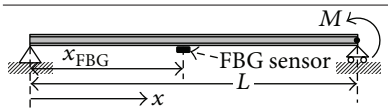	$0 < x_{FBG} \le L$	$\dfrac{x}{x_{FBG}}$
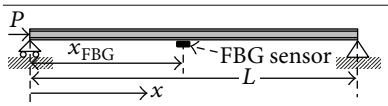	$0 < x_{FBG} \le L$	-1

strain caused by multiple loadings can be found by setting the derivative of (6) equal to zero:

$$\frac{d}{dx}\left(\sum_{j=1}^{n}\lambda_j^k\phi_j^k(x)\right) = 0. \tag{9}$$

3.3. Example Case: Simply Supported Beam Subjected to Three Types of Loads. To measure the strains in the beam structure subjected to a uniformly distributed load F_1 and two end moments F_2 and F_3, three FBG sensors are attached at three different locations, as shown in Figure 4.

3.3.1. Strain-Shape Functions and Total Strain. The total strain distribution of the beams in Figure 4 is found by superimposing the strains caused by the three different loadings acting separately. If the first FBG sensor is selected to calculate the strain-shape functions and participation factors, the strain-shape functions for the three different loadings of F_1, F_2, and F_3 can be found in the first, fourth, and fifth rows of Table 1, respectively. The strain-shape functions are given by

$$\phi_1^1(x) = \frac{x(L-x)}{x_1(L-x_1)},$$
$$\phi_2^1(x) = \frac{L-x}{L-x_1}, \tag{10}$$
$$\phi_3^1(x) = \frac{x}{x_1}.$$

From (8), the participation factors for the three loadings λ_1^1, λ_2^1, and λ_3^1 can be found by

$$\begin{Bmatrix} \lambda_1^1 \\ \lambda_2^1 \\ \lambda_3^1 \end{Bmatrix} = \begin{bmatrix} \dfrac{x_1(L-x_1)}{x_1(L-x_1)} & \dfrac{L-x_1}{L-x_1} & \dfrac{x_1}{x_1} \\ \dfrac{x_2(L-x_2)}{x_1(L-x_1)} & \dfrac{L-x_2}{L-x_1} & \dfrac{x_2}{x_1} \\ \dfrac{x_3(L-x_3)}{x_1(L-x_1)} & \dfrac{L-x_2}{L-x_1} & \dfrac{x_3}{x_1} \end{bmatrix}^{-1} \begin{Bmatrix} \varepsilon_1 \\ \varepsilon_2 \\ \varepsilon_3 \end{Bmatrix}. \tag{11}$$

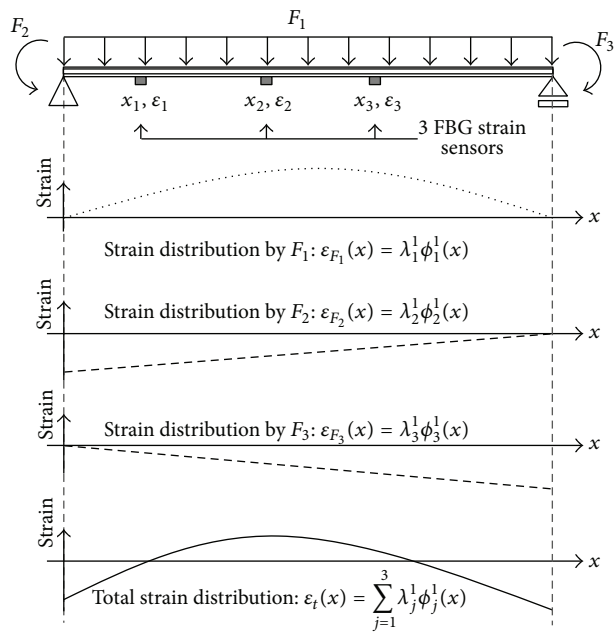

Figure 4: Distribution of the strain-shape functions for a beam subjected to three different loadings.

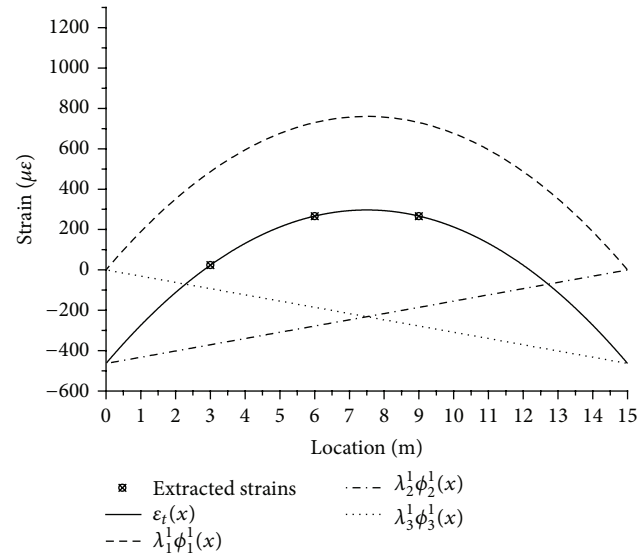

Figure 5: Composition of the total strain distribution.

Then, the total strain $\varepsilon_t(x)$ at an arbitrary location is found by substituting λ_1^1, λ_2^1, λ_3^1, $\phi_1^1(x)$, $\phi_2^1(x)$, and $\phi_3^1(x)$ into (6):

$$\varepsilon_t(x) = \sum_{j=1}^{3}\lambda_j\phi_j^1(x) = \lambda_1\frac{x(L-x)}{x_1(L-x_1)} + \lambda_2\frac{L-x}{L-x_1} + \lambda_3\frac{x}{x_1}. \tag{12}$$

3.3.2. Maximum Strain. Using the total strain distribution along the length of a beam structure in (12), the location for the maximum strain caused by the three loadings can be found by setting the derivative of (12) equal to zero:

$$\frac{d}{dx}\varepsilon_t(x) = \lambda_1^1\frac{L-2x}{x_1(L-x_1)} - \lambda_2^1\frac{1}{L-x_1} + \lambda_3^1\frac{1}{x_1} = 0. \tag{13}$$

Then, the solution of (13), x^*, is found by

$$x^* = \frac{L}{2} - \frac{\lambda_2^1}{\lambda_1^1}\frac{x_1(L-x_1)}{2(L-x_1)} + \frac{\lambda_3^1}{\lambda_1^1}\frac{x_1(L-x_1)}{2x_1}. \tag{14}$$

Therefore, the maximum strain can be obtained by comparing (1) the strain calculated by substituting x^* into x in (12) and (2) the strains at both ends of the beam.

3.3.3. Simulation of the Example Case. To test the performance of the measurement model, the intensities of the three loadings F_1, F_2, and F_3 acting on the steel beam in Figure 4 are set to 37.1, −636.0, and 636.0 kNm, respectively. For the simulation, H-708×302×15×28 was used for the section of the beam structure, and three FBG sensors were attached 3, 6, and 9 m from the left-hand end of the beam. From the structural analysis for the beam structure, the strains for FBG #1, #2, and #3 were found to be 23.2, 266.6, and 266.6 $\mu\varepsilon$, respectively.

Using the values of the strains for FBG #1, #2, and #3, the participation factors of λ_1^1, λ_2^1, and λ_3^1 in (11) were calculated as 486.6, −370.7, and −92.7, respectively. Thus, the total strain of the beam $\varepsilon_t(x)$ in (12) is expressed as

$$\begin{aligned}\varepsilon_t(x) = \sum_{j=1}^{3}\lambda_j^1\phi_j^1(x) &= (486.6)\left(-\frac{x^2+15x}{36}\right)\\ &\quad + (-370.7)\left(-\frac{x-15}{12}\right) + (-92.7)\left(\frac{x}{3}\right).\end{aligned} \tag{15}$$

The distributions of the total strains and the strains caused by the three loadings are plotted in Figure 5, which illustrates that the strain values for FBG #1, #2, and #3 obtained from the structural analyses are identical to those estimated by the measurement model.

The influence ratio R_j is defined in (16) to identify the influence of each loading on the value of the total strain:

$$R_j = \frac{\int_0^L \lambda_j^k\phi_j^k(x)\,dx}{\sum_{i=1}^{n}\sqrt{\left(\int_0^L \lambda_i^k\phi_i^k(x)\,dx\right)^2}}. \tag{16}$$

The influence ratio R_j indicates a ratio of the area of the strain distribution caused by the jth loading to the sum of the areas of the strain distributions caused by n different loadings. If the influence ratio R_j has a positive sign, then R_j has the same sign as the total strain distribution. Furthermore, the sum of the absolute values of the influence ratios must be one. Thus, the influence of each loading on the total strain distribution can be checked by the influence ratio proposed here. Table 3 presents the strain-shape functions, participation factors, and influence ratios for this simulation for three different FBG sensor numbers ($k = 1, 2$, and 3). For this example case, the most active loading is the uniformly distributed loading of F_1.

Table 2: Distributional strain-shape function $\phi(x)$: cantilever beam.

Loading condition	Condition of FBG sensor location	$\phi(x)$
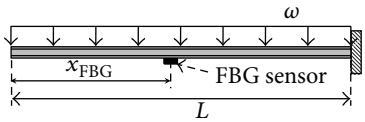	$0 < x_{FBG} \leq L$	$\frac{x^2}{x_{FBG}{}^2}$
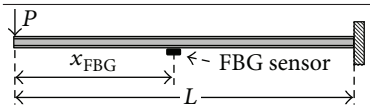	$0 < x_{FBG} \leq L$	$\frac{x}{x_{FBG}}$
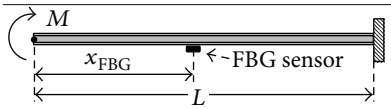	$0 < x_{FBG} \leq L$	1

Table 3: The function of the total strain distribution and its components.

Load	$k = 1$		$k = 2$		$k = 3$		$\lambda_j^k \phi_j^k(x)$	R_j
	λ_j^k	$\phi_j^k(x)$	λ_j^k	$\phi_j^k(x)$	λ_j^k	$\phi_j^k(x)$		
F_1	486.6	$-(x^2 - 15x)/36$	730.0	$-(x^2 - 15x)/54$	730.0	$-(x^2 - 15x)/54$	$-13.52(x^2 - 15x)$	0.522
F_2	−370.7	$-(x - 15)/12$	−278.0	$-(x - 15)/9$	−185.4	$-(x - 15)/6$	$-30.89(x - 15)$	−0.239
F_3	−92.7	$x/3$	−185.4	$x/6$	−278.0	$x/9$	$-30.89(x)$	−0.239
$\varepsilon_t = \sum_{j=1}^{3} \lambda_j^k \phi_j^k(x) = -13.52(x^2 - 15x) - 30.89(x - 15) + 30.89(x)$								

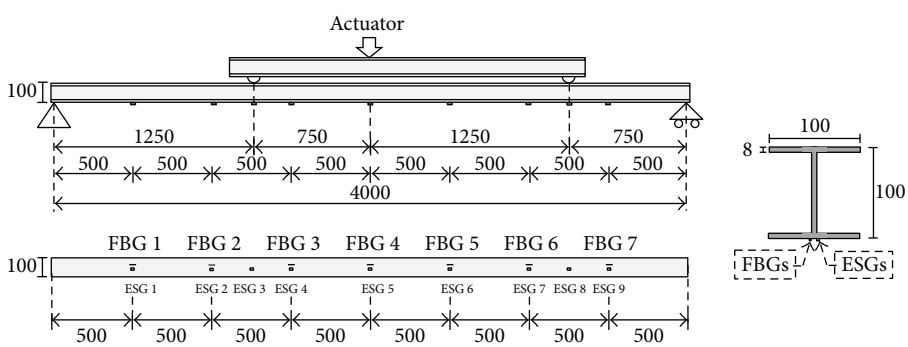

(a) Side and bottom views for the test model subjected to two point loadings

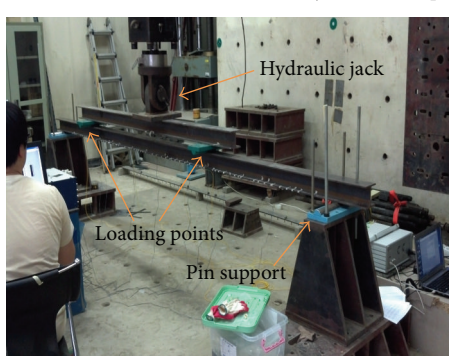

(b) Overall view of the test model

Figure 6: Test model setup.

4. Application to Measurements of the Maximum Strain of a Steel Beam

The proposed measurement model could evaluate the maximum strain in beam structures subjected to multiple loading conditions using the strain-shape functions for various loadings, including point loading, distributed loading, and bending moment loading, as shown in Tables 1 and 2. The proposed measurement model was demonstrated for distributed loading and bending moment loading by a numerical simulation in Section 3.3. In this chapter, the experimental test is conducted to evaluate the performance of the proposed measurement model for the point loading condition.

4.1. Test Setup. In the bending test of the simply supported steel beam in Figure 6, a concentrated load was applied on the upper steel beam by a hydraulic jack. The load was increased in two steps, 7.4 and 12.9 kN. The concentrated load was split into two concentrated loads applied 1.25 and 3.25 m from the left end of the beam. The section of the beams was H-100 × 100 × 6 × 8 with a length of 4 m. Figure 6(a) shows that the measurements during the bending test were performed with both seven FBG sensors with a 10 mm grating length and nine ESGs with a 5 mm gauge length attached to the surface of the bottom flange. IS 7000, which is manufactured by Fiberpro, was used for the interrogation system. The major specifications of IS 7000 are listed in Table 4. The grating lengths of the seven FBG sensors are 1,540–1,560 nm, in accordance with the wavelength tuning range of IS 7000. The sampling rate for the strain measurement was set as 0.1 per second.

4.2. Results. During the test, the beam deflected downward and tensile longitudinal strains occurred at the outer surface of the bottom flange. Before testing the measurement model, the strains obtained from the FBGs and ESGs were compared to verify the quality of the value by the FBGs. Table 5 indicates that the strain measured by FBGs could be assessed as reliable values for sensing beam members. The maximum difference between the two measurements was found to be less than 1.34% for each load step.

To measure the maximum strain of the test model subjected to two different point loads, two FBG sensors were required to estimate the maximum strain of the beam based on the model proposed in (6). Among the 21 possible combinations when choosing two of the seven FBG sensors without repetition, the combination of the first and second FBG sensors attached 0.5 and 1.0 m from the left end of the beam is not valid for the estimation because the matrix $[\phi^k]$ in (8) based on the combination is singular.

To test the dependency on the selection of the locations for FBG sensors in the measurement of the maximum strain, all 20 FBG sensor combinations in Table 6 were used in the measurements. The numbers for the FBG sensors are shown in Figure 6(a). Figure 7 compares the estimated distributions of strains from the 20 FBG sensor combinations with the strains measured directly from the nine ESGs for each loading step. Furthermore, the dependency of the locations for the FBG sensors installed at the beam structure on the selection can be avoided using the measurement model in (5).

Table 4: Major specifications of the interrogator (IS 7000).

Laser module (wavelength swept laser)	
Wavelength tuning range	1,533.7–1,569.5 nm
Sensor module	
Repeatability	±2 pm
Wavelength accuracy	<±10 pm
Sampling frequency	200 Hz

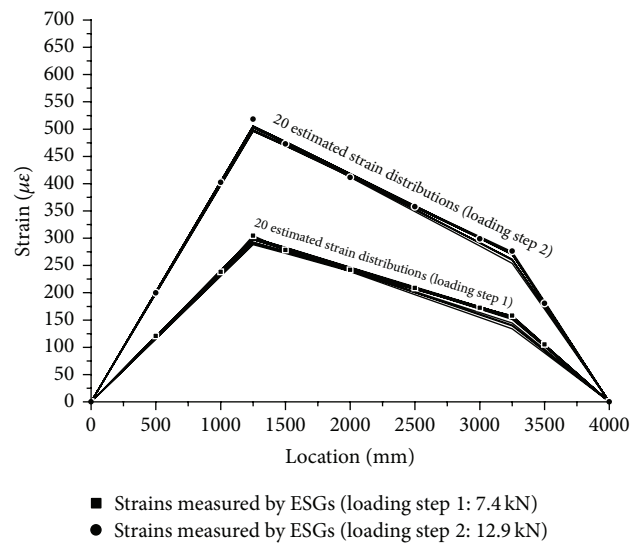

Figure 7: Estimated strain distributions from different combinations of FBG sensors for two.

To evaluate the performance of the measurement model, the relative error in the estimated strain distributions was calculated by

$$\text{relative error of strain distribution } (\%) = \frac{\left\|\varepsilon_{\text{est}} - \varepsilon_{\text{ESG}}\right\|}{\left\|\varepsilon_{\text{ESG}}\right\|} \times 100, \tag{17}$$

where ε_{ESG} is a vector of the strains measured directly from nine ESGs and ε_{est} is a vector of the estimated strains from the model. Figure 8 indicates that the average relative errors for the 20 possible combinations of strain distributions are 2.37% and 1.84% for loading steps 1 and 2, respectively. The maximum of the relative errors for all combinations was approximately 6% for the first combination in load step 2. The estimated maximum strains based on the 20 combinations are compared with the maximum directly measured from ESG #3 in Figure 9. The average relative errors for the 20 possible combinations in the maximum strain are 2.54% and 2.74% for loading steps 1 and 2, respectively. The experimental results indicate good agreement between the estimated strains based on the model and the strains measured from the ESGs.

Table 5: Measured strain by the FBG sensors and ESGs.

Sensing location (mm)	First step (7.4 kN)			Second step (12.9 kN)		
	FBG ($\mu\varepsilon$)	ESG ($\mu\varepsilon$)	Relative error (%)	FBG ($\mu\varepsilon$)	ESG ($\mu\varepsilon$)	Relative error (%)
500	120.5	120.9	0.36	202.2	199.6	1.34
1,000	238.4	238.3	0.01	405.2	402.6	0.64
1,250	—	304.6	—	—	518.1	—
1,500	280.3	278.3	0.74	474.9	472.8	0.45
2,000	240.4	241.8	0.57	413.8	411.4	0.59
2,500	207.2	208.7	0.69	358.3	357.9	0.10
3,000	172.7	172.3	0.22	299.7	299.0	0.24
3,250	—	157.9	—	—	276.5	—
3,500	104.1	105.3	1.16	181.0	180.6	0.21

Table 6: Number alignment of the combinations.

Combination number	1	2	3	4	5	6	7	8	9	10
Combination of sensors	(1,3)	(1,4)	(1,5)	(1,6)	(1,7)	(2,3)	(2,4)	(2,5)	(2,6)	(2,7)
Combination number	11	12	13	14	15	16	17	18	19	20
Combination of sensors	(3,4)	(3,5)	(3,6)	(3,7)	(4,5)	(4,6)	(4,7)	(5,6)	(5,7)	(6,7)

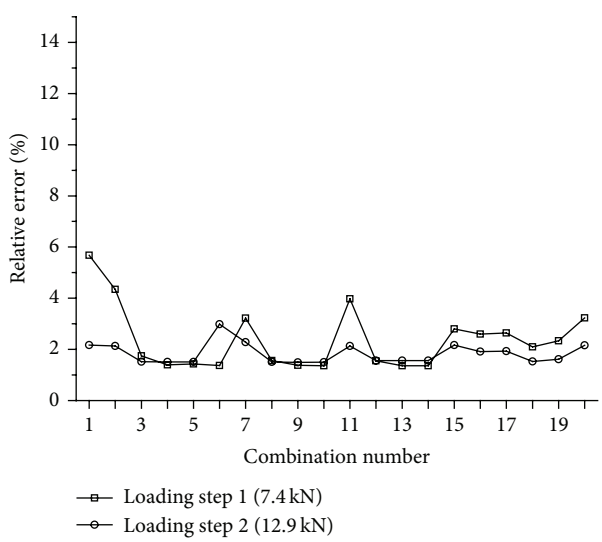

Figure 8: Relative errors of the estimated strain distributions.

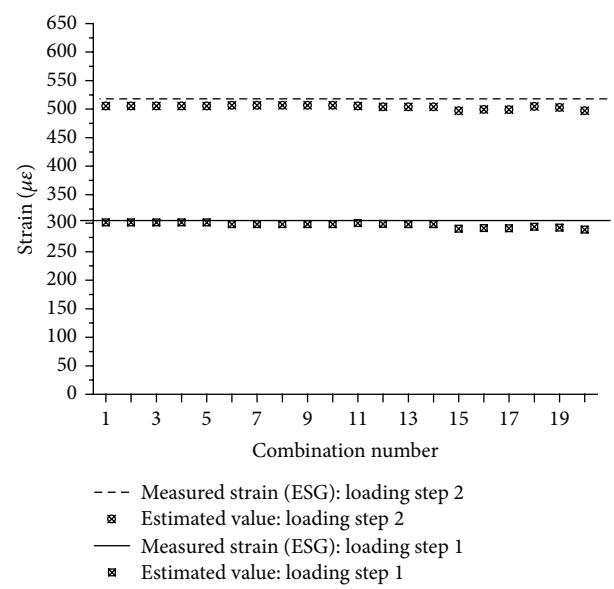

Figure 9: Maximum strains estimated from the estimated strain distributions.

5. Conclusion

In this paper, a maximum strain measurement model for beam structures subjected to multiple loading conditions is developed by defining the strain-shape function and participation factors. The maximum strain in a beam is found by the sum of the strains caused by the different loadings acting separately. The strain-shape functions for various loading and support conditions are derived, and a system of equations is defined to calculate the participation factors. The influence of each loading on the value of the total strain can be identified using the influence ratio defined here.

The measurement model is applied to monitor the maximum strain in a 4 m long steel beam subjected to two concentrated loads. Seven FBG sensors and nine ESGs were attached on the surface of the bottom flange to obtain measurements during the test. The estimated maximum strain and distribution of strains along the length of the beam were compared with those obtained directly from the ESGs. The experimental results indicate good agreement between the strains that were estimated based on the model and the strains measured by the ESGs. Furthermore, the dependency of the locations for the FBG sensors installed on the beam structure on the selection can be avoided using the measurement model.

Acknowledgments

This research is supported by Grant (code #09 R&D A01) from High-Tech Urban Development Program funded by the Ministry of Land, Infrastructure and Transport.

References

[1] AISC, *Manual of Steel Construction, Allowable Stress Design*, American Institute of Steel Construction, Chicago, Ill, USA, 1989.

[2] H. S. Park, H. M. Lee, H. Adeli, and I. Lee, "A new approach for health monitoring of structures: terrestrial laser scanning," *Computer-Aided Civil and Infrastructure Engineering*, vol. 22, no. 1, pp. 19–30, 2007.

[3] Y. Wang, Y. Wang, Y. Li, J. Ran, and M. Cao, "Experimental investigation of a self-sensing hybrid GFRP-concrete bridge superstructure with embedded FBG sensors," *International Journal of Distributed Sensor Networks*, vol. 2012, Article ID 902613, 10 pages, 2012.

[4] T. H. Yi and H. N. Li, "Methodology developments in sensor placement for health monitoring of civil infrastructures," *International Journal of Distributed Sensor Networks*, vol. 2012, Article ID 612726, 11 pages, 2012.

[5] H. S. Park, H. S. Jung, Y. H. Kwon, and J. H. Seo, "Mathematical models for assessment of the safety of steel beams based on average strains from long gage optic sensors," *Sensors and Actuators A*, vol. 125, no. 2, pp. 109–113, 2006.

[6] T. A. Hampshire and H. Adeli, "Monitoring the behavior of steel structures using distributed optical fiber sensors," *Journal of Constructional Steel Research*, vol. 53, no. 3, pp. 267–281, 2000.

[7] H. S. Park, S. M. Jung, H. M. Lee, Y. H. Kwon, and J. H. Seo, "Analytical models for assessment of the safety of multi-span steel beams based on average strains from long gage optic sensors," *Sensors and Actuators A*, vol. 137, no. 1, pp. 6–12, 2007.

[8] H. M. Lee and H. S. Park, "Gage-free stress estimation of a beam-like structure based on terrestrial laser scanning," *Computer-Aided Civil and Infrastructure Engineering*, vol. 26, no. 8, pp. 647–658, 2011.

[9] K. T. V. Grattan and T. Sun, "Fiber optic sensor technology: an overview," *Sensors and Actuators A*, vol. 82, no. 1, pp. 40–61, 2000.

[10] S. W. James, M. L. Dockney, and R. P. Tatam, "Simultaneous independent temperature and strain measurement using in-fibre Bragg grating sensors," *Electronics Letters*, vol. 32, no. 12, pp. 1133–1134, 1996.

[11] H. Li, D. Li, and G. Song, "Recent applications of fiber optic sensors to health monitoring in civil engineering," *Engineering Structures*, vol. 26, no. 11, pp. 1647–1657, 2004.

[12] D. Luo, Z. Ibrahim, Z. Ismail, and B. Xu, "Optimization of the geometries of biconical tapered fiber sensors for monitoring the early-age curing temperature of concrete specimens," *Computer-Aided Civil and Infrastructure Engineering*, vol. 28, no. 7, pp. 531–541, 2013.

[13] M. Mieloszyk, L. Skarbek, M. Krawczuk, W. Ostachowicz, and A. Zak, "Application of fibre Bragg grating sensors for structural health monitoring of an adaptive wing," *Smart Materials and Structures*, vol. 20, Article ID 125014, 12 pages, 2011.

[14] R. C. Tennyson, A. A. Mufti, S. Rizkalla, G. Tadros, and B. Benmokrane, "Structural health monitoring of innovative bridges in Canada with fiber optic sensors," *Smart Materials and Structures*, vol. 10, no. 3, pp. 560–573, 2001.

[15] W. Chung and D. Kang, "Full-scale test of a concrete box girder using FBG sensing system," *Engineering Structures*, vol. 30, no. 3, pp. 643–652, 2008.